Microporous and Mesoporous Materials 226 (2016) 44–52

Contents lists available at ScienceDirect

Microporous and Mesoporous Materials

journal homepage: www.elsevier.com/locate/micromeso

Mechanical characterization of aerogel materials with digital image correlation

Rami Haj-Ali [a], Rami Eliasi [a], Victor Fourman [a], Chen Tzur [a], Galit Bar [b], Eitan Grossman [c], Ronen Verker [c], Raz Gvishi [b], Irina Gouzman [c], Noam Eliaz [d, *]

[a] School of Mechanical Engineering, Tel-Aviv University, Ramat Aviv, Tel Aviv 6997801, Israel
[b] Applied Physics Division, Soreq NRC, Yavne 81800, Israel
[c] Space Environment Department, Soreq NRC, Yavne 81800, Israel
[d] Department of Materials Science and Engineering, Tel-Aviv University, Ramat Aviv, Tel Aviv 6997801, Israel

ARTICLE INFO

Article history:
Received 29 March 2015
Received in revised form
1 December 2015
Accepted 17 December 2015
Available online 29 December 2015

Keywords:
Silica aerogels
Mechanical properties
Digital image correlation
Disk compression
Inverse mechanics

ABSTRACT

Silica aerogels are ultralow density materials with nano-sized skeleton network of pores. Their high brittle nature presents a major challenge for mechanical testing and a need exists for novel testing methods. Two new mechanical setups and testing techniques are proposed for measuring the aerogel elastic mechanical properties. Both techniques employ full-field Digital Image Correlation (DIC) for surface deformation measurements. The first setup uses disk compression experiment, known as diametral compression test (Brazilian disk). However, the elastic properties of the material cannot be obtained directly. Instead, an inverse mechanics computational scheme, using both a finite element (FE) model and analytical solution, is proposed. The second direct testing setup is uniaxial compression of rectangular-shaped blocks. The Young's modulus and Poisson's ratio are extracted directly from the experimental stress–strain curves. Our results of tested samples show the relation between the density and the Young's modulus to coincide with previously published trends. The direct and iterative inverse-mechanics solution methods agree well with each other. The Poisson's ratio is found to be independent of the material apparent density. Comparisons between the two methods and recommendations for expanding the disk testing approach to fracture toughness are discussed.

© 2015 Elsevier Inc. All rights reserved.

1. Introduction

Aerogels comprise a special class of low-density open-cell solid foams (typically, with porosity over 90%) which exhibit many unique properties such as exceptionally lightweight, high surface area, low thermal conductivity, extremely low dielectric constant, low sound wave transmission, high optical transparency in a wide range of wavelengths close to that of glass, and a very low refractive index [1–4]. These properties result from the microstructure of aerogels, which consists of a three-dimensional amorphous solid skeleton network with interconnected nanometer-sized pores in between. Silica aerogels are used for thermal and electrical insulation, especially in space applications, oxygen and humidity sensors, aerosol particle collectors, space mirror protectors, catalyst supports, battery electrodes, *etc.* [5].

The structure of the aerogel is sponge-like with nano-structured airy material whose three-dimensional network of interconnected silica particles forms cylindrical and branched open 2–50 nm pores. The elastic modulus of highly porous aerogel materials is proportional to the relative density raised by the m^{th} power ($3 \leq m \leq 4$). Ma et al. [6] proposed a computational model using diffusion-limited cluster–cluster aggregation (DLCA) algorithms along with FE models to estimate the elastic properties. Their computational modeling resulted in $m \approx 3.6$ for perfectly connected micro-structures.

In general, aerogels are highly brittle materials, although they can have a high stiffness-to-density ratio. Due to their low toughness, there is a major challenge to perform mechanical tests with these materials. Characterization of the mechanical properties of aerogels is important in order to design engineering applications and utilize their unique physical properties. Woignier et al. [7–9] performed both three-point bending and acoustical experiments in order to determine the static and the dynamic Young's moduli,

* Corresponding author. Tel.: +972 (3) 640 7384; fax: +972 (3) 640 6648.
E-mail address: neliaz@tau.ac.il (N. Eliaz).

http://dx.doi.org/10.1016/j.micromeso.2015.12.035
1387-1811/© 2015 Elsevier Inc. All rights reserved.

respectively, of monolithic parallelepipedic non-densified silica aerogel samples. It was found that the density dependence of the Young's modulus, E, can be scaled by a power-law function $\phi^{3.8}$, where ϕ is the volume fraction, so a calibration law was proposed accordingly. Dynamic experiments have been carried out by means of the Brillouin scattering acoustic technique [7,10]. The longitudinal and transverse wave-length velocities were measured, allowing the determination of the elastic constants. Woignier and Phalippou [8] further extended the three-point bending method for densified aerogels. A general trend in which E increases with the density was observed, with E values varying between 10^{-3} and 10^{-2} GPa. Two different slopes with two different scaling exponents were observed. Thus, it was deduced that non-densified aerogels and densified aerogels have different elastic behaviors. The mechanical strength of silica aerogels has also been determined by bending tests [8].

Gross et al. [11] employed ultrasonic and static compression experiments at high frequencies in which longitudinal and transverse velocities were measured for different densities of aerogels. The Poisson's ratios thus determined were not affected by the density variations. Tillotson and Hrubesh [12] investigated the mechanical properties of ultralow-density aerogels (3–80 mg/cm^3). Scattered results for densities lower than 80 mg/cm^3 were shown since measurement in this range of low densities was more difficult to implement. The results coincided with previously published results reflecting a lower power-law slope for the ultralow-density aerogels compared with the higher-density silica aerogels. Scherer et al. [13,14] measured the shear modulus and bulk modulus of alkoxide-derived silica gels during aging and drying stages.

Parmenter and Milstein [15] investigated the mechanical behavior of fiber-reinforced and unreinforced silica aerogels using indentation and block compression tests. The direct (block) compressive strength showed correlation with the hardness results. Moner-Girona et al. [16] investigated the mechanical properties of silica aerogels by means of the micro-indentation technique. The Young's modulus for the lightest aerogel (80 mg/cm^3) was 7.0 MPa, whereas the highest density (260 mg/cm^3) yielded a modulus of 346 MPa. The four experimental points were fitted according to power-law function for the Young's modulus, with a power $\alpha = 3.0\pm0.2$. Wong et al. [17] investigated the elastic modulus of a wide range of hydrophobic silica aerogels in order to study the effect of density on modulus, which ranged from 40 kPa to 70 MPa. Tension and compression tests along with thermal conductivity properties were also reported. The Brazilian disk test was used for the limited purpose of measuring the tensile strength only.

To-date, very few studies have used Digital Image Correlation (DIC) for aerogels. Sun et al. [18] established guidelines for preparing shear tests of ceramic-fiber-reinforced aerogel. Iosipescu aerogel specimens with two different notches were investigated using the FE method. It was proposed (without actually applying it) that the needed mid-section strain gages can be replaced by the DIC method. Dynamic compressive tests of cross-linked silica aerogel using a split Hopkinson pressure bar (SHPB) were conducted by Luo et al. [19]. The DIC method was employed using high-speed image acquisition. The Poisson's ratio was determined to be 0.162. Ductile splitting was observed at high strain rates, but the samples were much more ductile than native silica aerogels. Luo et al. [20] studied the mechanical properties of isocyanate-crosslinked vanadia aerogels under both quasi-static loading conditions and high strain rate loading conditions using a SHPB. DIC was used to measure the surface strains, indicating nearly uniform compression at all stages of deformation during compression. In our study we apply the DIC method in a unique fashion and demonstrate the use of virtual extensometer (extension or shortening distance between two points). There are strong reasons for using the proposed DIC for aerogels. The latter are brittle, and contact gauges for deformation measurements cannot be mounted without local damage. In addition, the full-field nature of the DIC allows both overall and local strain measurements, including of the Poisson's ratio. The DIC can also be used for inhomogeneity, damage and flow detections.

Fracture toughness tests using the Single-Edge-Notched Beam (SENB) technique have been conducted [9], showing that for aerogel samples having densities between 0.1 and 0.35 g/cm^3, the fracture toughness K_{IC} ranges between 0.8 and 4.8 KPa-m$^{1/2}$ and can be scaled by a power law with an exponent equals to 1.6±0.2. Alaoui et al. [21] measured the toughness of alcogels and aerogels with different porosities by SENB. The mechanical strength was also measured using the three-point bending on un-notched specimens. Both aerogel and alcogel samples were monolithic with densities ranging from 90 to 250 mg/cm^3. It was observed that, for a given density, the toughness of aerogels was higher (by a factor close to 2) than alcogels. This toughness enhancement is expected taking into account the textural and structural transformation of the gel, and was attributed to the growth of the necks between the particles.

The brittle nature of the light-weight aerogel presents several challenges for mechanical testing, such as end fixtures for mounting the specimen, contact method for applying the load, and displacement measurements during the test up to ultimate failure. Standard deformation measurement techniques (*e.g.* strain gauges, extensometers) are found unsuitable since they cause damage to the specimen. Therefore, non-contact optical measurement techniques offer a better alternative for monitoring the deformation during loading. In this study, we examine the use of the optical two-dimensional (2D) DIC technique. The 2D-DIC technique is a full-field non-contact optical technique for spatial deformation measurement on the surface of the tested sample. It directly provides the displacement components on the surface. The 2D-DIC computational algorithm divides the measured area into cells and tracks and compares features to locate their displacement vectors with time from a successive series of digital images. The DIC method has been extensively developed and applied since the early 1980's, and its principles and theoretical background have been extensively reported [22–26].

The overall objective of this work is to examine two new experimental tests and data characterization of light-weight silica aerogels in order to determine reliably their elastic properties, such as the Young's modulus. Direct block compression and indirect diametral (Brazilian disk) tests are employed. To the best of our knowledge, this is the first ever use of the Brazilian disk test for measuring the Young's modulus of aerogels. The non-contact full-field 2D-DIC strain measurement is used, and a technique is developed for applying an external coat with speckle field. A back-calculation (inverse mechanics) technique is used in the indirect tests to determine the mechanical properties of aerogels from the test results and parametric finite-element solutions.

2. Experimental

2.1. Materials and samples characterization

The tested silica aerogel samples were in the form of disks and blocks with dimensions of about 2.6 cm × 0.7 cm and 2.5 cm × 2.5 cm × 1.0 cm, respectively. These samples were obtained commercially from Aerogel Technologies™ [27]. They are hydrophilic and were supercritically dried with CO_2. Each sample was labeled 'compression aerogel disk (CAD)' followed by its number. Therefore, the first task was to perform geometrical

measurements by means of digital pictures of each specimen. These pictures were acquired by a FinePix S100FS Fujifilm camera, with a resolution of 11.1 megapixels, in a super-macro mode. For calibration purposes, a millimetric paper was placed in a parallel manner, adjacent to the specimen's surface, in the plane closest to the camera. As can be seen from Fig. 1, the thickness of the disk is not completely uniform. In addition, it is worth noting that all disk samples possess a concave shape. All geometry measurements were carried out using National Instruments' Vision Assistant 8.0 (2005) [28]. All specimens were weighed using Vibra's AJH-620CE electronic balance, having a range between 0.1 and 620 g and accuracy of 1 mg. The obtained weight and volume were used to calculate the density of each sample. Table 1 reports the geometry and calculated density of the disk samples, with reference to their nominal values set by the manufacturer as 27 mm by 7 mm. It also reports similar results for the aerogel block samples with reference to their nominal values (25 mm × 25 mm × 10 mm). Large relative variations can be seen in the reported values. These may be due to the hydrophilic nature of the aerogel specimens, as they tend to experience shrinkage due to capillary stresses caused by residual adsorbates on their surface. Therefore, it is expected that the final dimensions will differ and be smaller than those provided as nominal values. The hydrophilic aerogel tends to accumulate humidity, which causes shrinkage and a density increase.

2.2. Surface preparation and digital image processing

The LaVision DIC system [29] is used in this study along with its Davis post processing and numerical computing software. A random gray intensity pattern is applied onto the aerogel surface in order to calculate the surface deformation by the 2D-DIC. The natural texture of a specimen often provides a sufficient random gray intensity distribution without the need to apply an exterior coat. In our case of close to transparent aerogels, an artificial pattern is used by spraying paint or by scattering micron-size carbon particles onto the specimen surface. This aerogel specimen preparation includes a generation of random speckle pattern by spraying paints onto the specimen surface in two layers. One side of the specimen is entirely covered by first spraying a very delicate thin layer of white paint and, then, spraying black paint on top of the white background to achieve adequate contrast of the speckle pattern. According to the spray's manufacturer data, its major components are Acetone (36.0%), Propane (17.0%), Toluene (11.9%), Butane (8.0%), and Lt. Aliphatic Hydrocarbon Solvent (5.2%). Although the aerogel has a relatively hygroscopic behavior, we assume that the influence of the thin coat on the overall mechanical properties is negligible. Fig. 1 illustrates the disk and block samples before and after applying the surface coat, and the relative uniformity of the gray patterns.

The quality of the acquired images significantly affects the DIC results. The application of the DIC in the current setup requires the determination of different parameters related to image acquisition and post processing. The acquired image is divided into a grid of 1600 pixels in the loading direction and 1200 pixels in the transverse direction. Focus and light intensity for good image contrast are defined in each experiment as the speckle patterns differ from one sample to another. The camera exposure time is manually selected using the DIC software. The setup of these photography parameters yield a gray level histogram that is examined prior to performing the test in order to ensure pixel dispersion within the scale of different gray levels. Our applied DIC system includes a 12-bit depth gray camera yielding 4096 gray levels, where 0 and 4095 represent the full black and white levels, respectively. A wide histogram acquired prior to the test shows a good dispersion for the number of pixels within each gray level. Image calibration procedure is carried out once the gray-level histogram is deemed acceptable.

2.3. Mechanical testing setups

The experimental setup included an Instron-5582 screw-driven loading frame controlled by Bluehill's operating system. A load cell

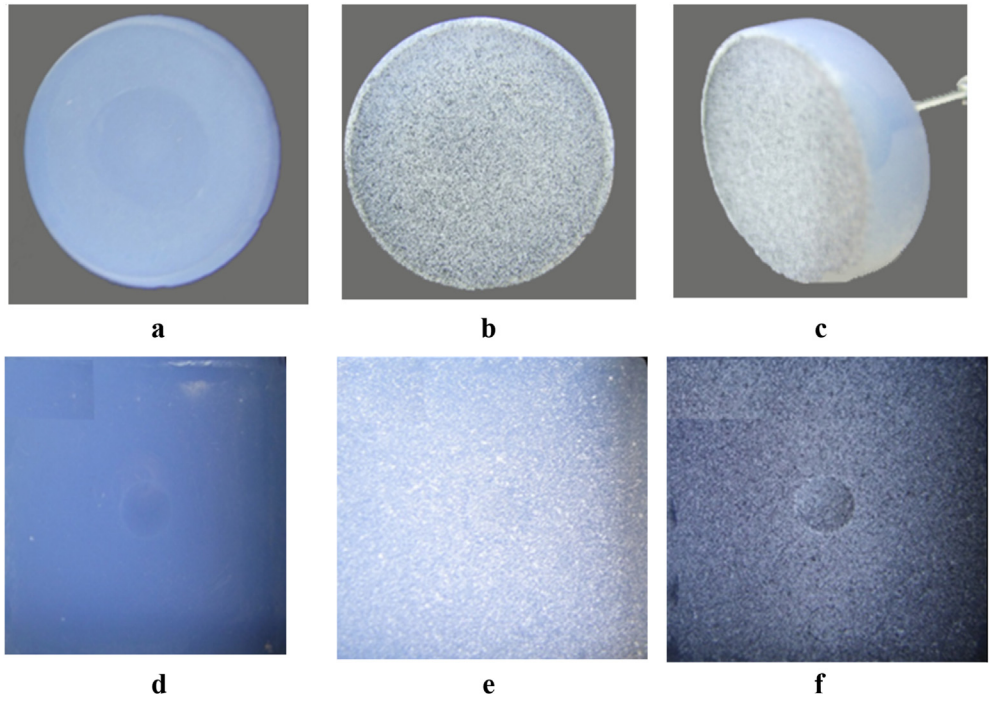

Fig. 1. Top row: aerogel surface preparation for the 2D-DIC measurement: (a) A specimen before the generation of random speckle pattern; (b) A front view of the speckle pattern; (c) Only one side of the specimen was entirely covered. Bottom row: an example of specimen's surface preparation, by stages, for 2D-DIC measurement for compression aerogel block CAB-6 specimen: (d) before spraying; (e) after spraying white paint; (f) after spraying black paint on top.

Table 1
Measured sample properties, geometry (diameter, thickness), mass and density, for ten disks. Right two columns list the Young's moduli (for assumed Poisson's ratios) obtained from the inverse mechanical scheme. Nominal geometry reported by the manufacturer: (~2.6 cm × 0.7 cm). Error is defined as the relative deviation from nominal to measured volumes.

Specimen label	$\bar{D}$ [mm]	$\bar{t}$ [mm]	Percentage error [%]	m [g]	ρ [g/cm^3]	E [MPa] $\upsilon = 0.2$	E [MPa] $\upsilon = 0.3$
CAD-1	25.32	7.08	4.00	0.65	0.181	2.78	2.78
CAD-2	24.65	8.79	12.90	0.67	0.159	2.41	2.40
CAD-3	24.73	7.71	0.37	0.59	0.159	2.90	2.89
CAD-4	26.18	8.05	16.57	0.70	0.161	2.81	2.81
CAD-5	24.06	7.69	5.89	0.65	0.184	3.19	3.19
CAD-6	25.10	6.80	3.54	0.61	0.171	3.62	3.62
CAD-7	24.00	7.88	4.05	0.69	0.194	3.64	3.64
CAD-8	25.20	6.95	6.74	0.67	0.192	4.76	4.76
CAD-9	25.12	6.99	6.75	0.67	0.193	4.63	4.62
CAD-10	24.73	7.37	4.70	0.64	0.182	4.37	4.36

with a maximum capacity of 100 N and accuracy of 0.5% of the measured load was used. A special fixture in the form of top and bottom plates (holders) for the disk samples was designed and self-manufactured in order to prevent disk rotation during the applied diametral compression. The load was applied through a displacement-control mode. The 2D-DIC setup was connected with the loading frame in order to accurately associate the images with the measured loads. The 2D-DIC system by LaVision consists of a CCD camera with a 12-bit depth and a spatial resolution of 1600 × 1200 pixels (about 2 megapixels). Image recording was simultaneously performed with the mechanical loading, supported by analog inputs from the test machine and the load cell data (*e.g.* force and displacement). In order to ensure in-plane deformation measurements, an alignment of the optical camera axis was carried out relative to the object surface. The specimen was uniformly illuminated by a fiber optics light source and flexible light tubes with variable intensities. All tests were carried out at ambient temperature with constant relative humidity.

Initially, the mechanical properties of ten aerogel disks were investigated using the diametral compression test (also known as Brazilian test) [30–33]. The Brazilian disk has more sensitivity to flaws than bending test due to the test configuration itself. Each sample was named 'CAD' followed by an ordinal number. In order to construct the proposed setup for aerogel disks, great efforts were made in order to develop improved setup, geometry and size. We initially used two samples with different materials, un-plasticized Polyvinyl Chloride (PVC-U) and classical sol–gel sample (~700 mg/cm^3), respectively. Rigid rotation of the disks was observed when the top flat loading surface was secured and fixed to the load cell. This rotation was minimized by using a brass compression fixture, shown in Fig. 2. The top portion of the fixture consisted of a flat plate with rounded half-slot made by milling disk cutter. The area designed to be in contact with the specimen had a concave surface, with a larger radius than the specimen to induce close to a point contact loading. It was also designed to be pin-connected to the crosshead. The bottom portion included a concave contact surface with a radius larger than that of the specimen. A vacuum pen was used to place the specimen, and a small pre-load was applied to keep the disk in contact with the top and bottom surfaces. The applied displacement rate was 1.0 mm/min.

The aim of this test is to extract the elastic properties. To this end, we first examine the classical elasticity solution, *e.g.* as in Ref. [34], of a disk under point loads. The displacement field is given by:

$$u(x,y) = -\frac{F_D}{4\pi\mu}\left\{(1-\kappa)tan^{-1}\left(\frac{2Rx}{x^2+y^2-R^2}\right) + \frac{(1-\kappa)x}{R} - \frac{4Rx(R^2-y^2+x^2)}{(R^2+x^2-2Ry+y^2)(R^2+x^2+2Ry+y^2)}\right\} \quad (1)$$

$$v(x,y) = -\frac{F_D}{4\pi\mu}\left\{\frac{(1+\kappa)}{2}ln\left(\frac{(R+y)^2+x^2}{(R-y)^2+x^2}\right) + \frac{(1-\kappa)y}{R} - \frac{8Rx^2y}{(R^2+x^2-2Ry+y^2)(R^2+x^2+2Ry+y^2)}\right\}$$

where F_D represents the compressive force per unit thickness, R is the radius of the circular disk, k is a constant that defines either plane stress ($k = \frac{3-\upsilon}{1+\upsilon}$) or plane strain ($k = 3-4\upsilon$) deformations, μ is the shear modulus, and υ is the Poisson's ratio. The solution is given in Cartesian coordinates with origin at the center of the disk. The elasticity solution is used to provide an estimated initial trial for the elastic properties. However, since we are not assuming plane deformation due to the finite thickness-to-diameter ratio, a 3D finite element (FE) model was generated to compare its solution with the DIC displacement fields for a given set of assumed elastic properties.

A 3D FE contact model is employed for each specimen, using the Abaqus general purpose implicit FE software [35] in order to simulate the experiments. The FE model consists of three parts, namely, a circular disk and two parallel rigid surfaces having contact with the disk. The mesh includes 6160 linear hexahedral elements of type C3D8R with 5 layers of elements through the thickness. The top rigid plate is allowed to move in contact downwards, but only along the vertical axis, while the bottom plate is fixed.

The computer simulation starts with an initial trial value of the aerogel modulus. Reaction force against the plate vertical displacement from the simulated model is compared with the test data. The latter consists of applied load that was derived from the loading frame against specimen shortening obtained from both the DIC and plate vertical movement. The inverse computational scheme consists of corrections of the estimated modulus until the linear portions of the two load-shortening curves are matched. The linear slope obtained by the FE simulation (initially, with assumed elastic properties) is compared to the experimental one. A new correction is applied to the Young's modulus and the FE is run again. The correction sign and magnitude depend on the sign and relative change in the current estimate between the load-deflection slopes. In case that the slope in the current run is larger than the previous one, the Young's modulus in the consequent FE run is decreased, and *vice versa*. This trial-and-error process is repeated until convergence. An extended inverse-mechanics scheme is developed by taking the FE converged results and correlating them with the 2D elasticity solution in order to extract an "improved" estimate of the material coefficients that appear in the elasticity solution. Once the load-deflection slope convergence is achieved, the displacements along horizontal and vertical diameters, u(x,0)

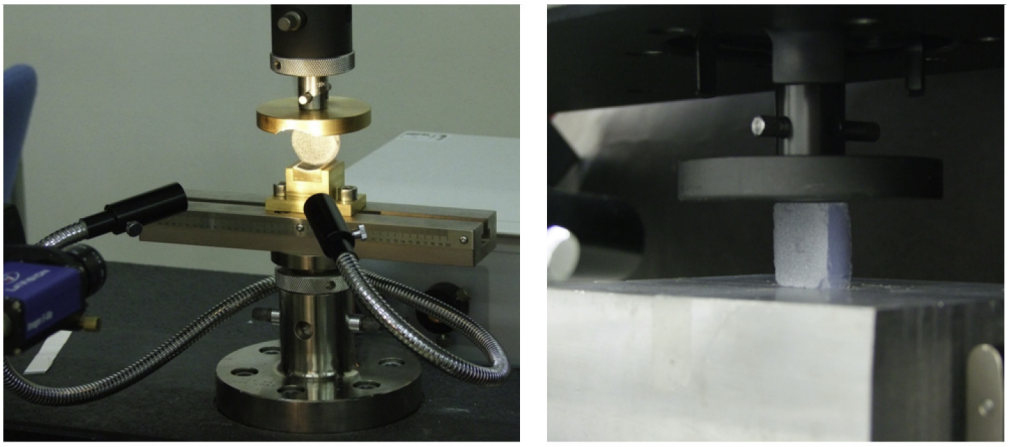

Fig. 2. (a) the 2D-DIC setup with a mounted camera in a fixed position in front of the aerogel specimen in the form of a disk. (b) Block compression mechanical testing setup.

and $v(0,y)$, respectively, are calculated. These are extracted from the FE results by means of discrete points along two defined paths.

A second mechanical testing setup was also developed for block aerogel samples. These samples are numbered and identified as compression aerogel block (CAB#). Unlike the disk setup, these block tests allow extracting the aerogel mechanical properties in a direct manner as a state of uniform compression stress and strain is imposed. Fig. 2b shows the block compression test setup. The loading frame procedure and sample preparation described for the disk samples are applicable for the block samples too. A flat loading surface is secured in its top portion to the load cell which ensures parallel top and bottom surfaces. The block specimen is placed between two parallel rigid surfaces for applying compressive load. All specimens are loaded at a constant crosshead moving velocity of 0.3 mm/min. The maximum vertical displacement depth was pre-determined to 3 mm downward, except for CAB-2 for which the maximum vertical displacement depth was pre-determined as 10 mm downward in order to reach failure. Finally, six aerogel block-shaped specimens were tested using this direct method and their mechanical properties were individually determined.

The sensitivity of the DIC technique decreases in the transverse direction as the displacement and strain associated with the Poisson's ratio are relatively smaller, hence higher resolution is needed in order to better resolve the strain and achieve reliable measurements. To this end, a second 2D-DIC system was used in this test in order to examine the accuracy of the first DIC system. The first disk experiments were carried out using a La-Vision CCD camera with a 12-bit depth and a spatial resolution of 1600 × 1200 pixels. Here, we added a second DIC system carried out by a PixeLINK PL-A686 CCD camera [36], with a 8-bit depth and a spatial resolution of 2208 × 3000 pixels (about 6.6 megapixels). A modular microscope, Navitar 12× Zoom with an adapter tube of 2× and a lens of 0.5×, was used to achieve a magnification range between 0.58× and 7.0×. The field of view was maximized by using the lowest magnification possible (0.58×), yielding a total magnification of 1.14. Both DIC data (*i.e.* from the 2- and 6-megapixel cameras) were processed *via* the Davis 7.4 and the VIC-2D [37] DIC post-processing commercial programs. Comparing the four combinations of DIC results allowed us to draw conclusions on the DIC setup. It was thus found that the selected magnification was sufficient for the determination of the Poisson's ratio. In addition, the lower spatial resolution of the La-Vision CCD camera in our Lab was found to be suitable. The pointwise full-field strain contours extracted from the DIC were also used to generate line and area (window) average strain metrics in order to give strain measures especially when the theoretical strain field solution is constant.

3. Results and discussion

In this section the results from the two types of mechanical tests will be discussed. Fig. 3 shows typical DIC displacement contours during a Brazilian disk test (sample CAD-6) superimposed on the photo of the test with the measured load level. It should be noted that DIC displacement field at the surface of the samples is representative of the displacements found inside the sample volume, both in the case of plane stress and in the case of plane strain. The

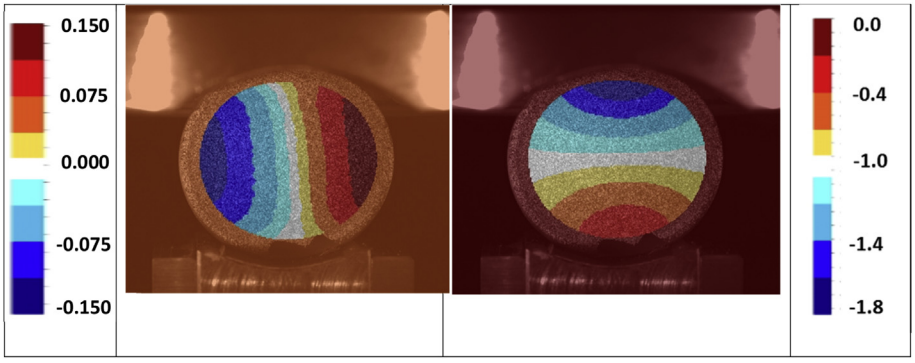

Fig. 3. Displacement fields obtained from the 2D-DIC processing of CAD-6 specimen: (left) in the *x*-direction; (right) in the *y*-direction. Legend contours for the displacement in mm scale.

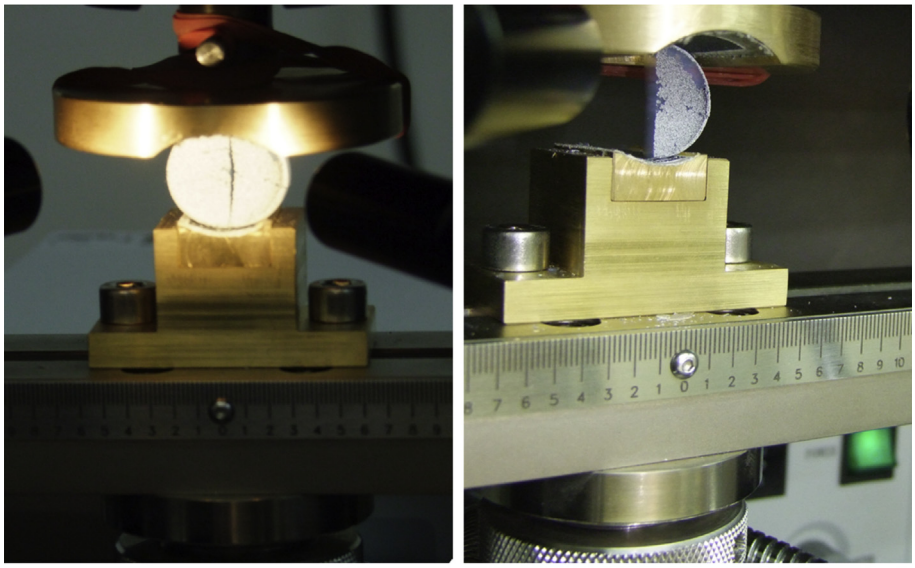

(a) (b)

Fig. 4. Typical disk compression setup showing: (a) specimen fractured along its vertical diameter; (b) a half-specimen after fracture failure.

displacement field is called a plane displacement and does not have a gradient in the thickness direction. Fig. 4 illustrates a case where the loading is increased up to the brittle failure expected in the form of a vertical crack emanating from the center of the sample. The load-shortening curve for CAD-6 sample is shown in Fig. 5. The deviation from a perfect linear displacement field (homogeneous strain) within the entire sample is related to two origins. The first is the geometrical intrusion shown on the surface of the sample in the form of cup-shaped cavity due to manufacturing imperfections. The second is due to the relatively small height-to-width ratio discussed in Section 3.1. Fig. 6 illustrates the 3D-FE mesh used in this study. The FE contact compression analysis was carried out assuming linear material behavior and small strains. The FE matched the experimental results only in the linear range of response past the initial contact stage (beyond 0.25 mm in Fig. 5). The DIC results for the mechanical tests were post-processed for about 15 loading steps. Similar FE simulation was carried out in an automated fashion with trial-and-error corrections for the Young's modulus until convergence. The error measured between the FE and DIC was in the form of the displacement differences along the *x* and *y* axes. The typical full-field DIC displacement results shown in Fig. 3 for CAD-6 sample correlate very well with the analytical elasticity and computational FE solutions. This is especially true in the mid-range linear response (Fig. 5) where it is free from the initial contact indentation type behavior (reaching full contact between the two concave-convex surfaces) and not too close to

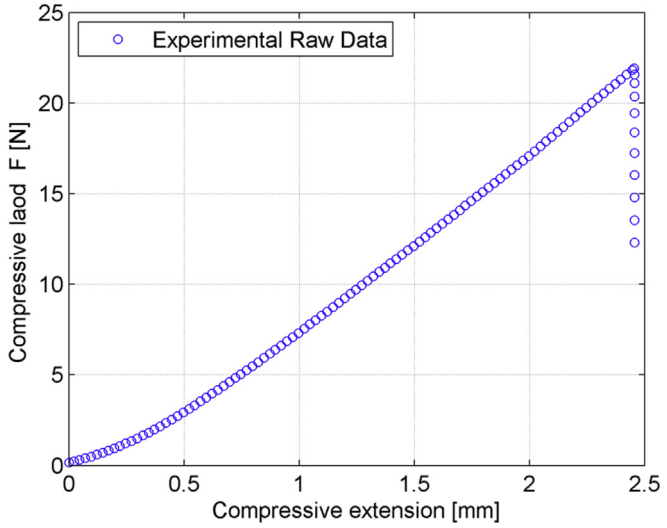

Fig. 5. Load-shortening data from compression test of CAD-6 sample up to ultimate failure.

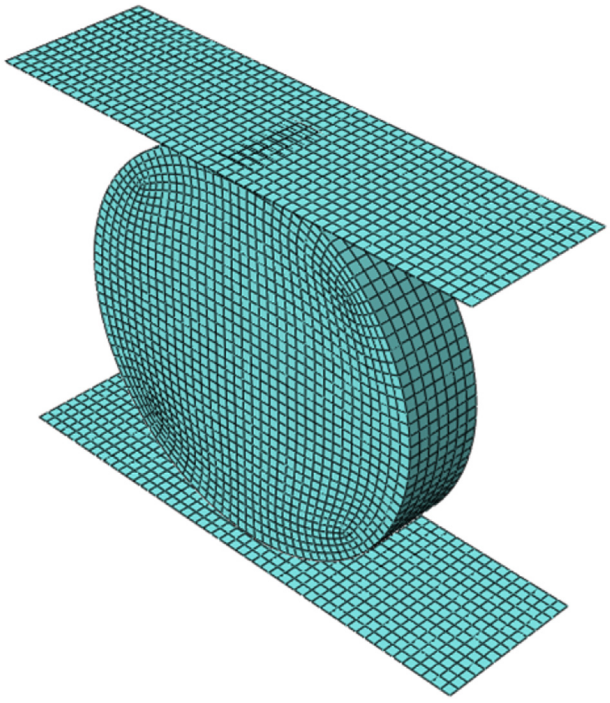

Fig. 6. Typical three-dimensional FE model for each tested disk along with two contact surfaces.

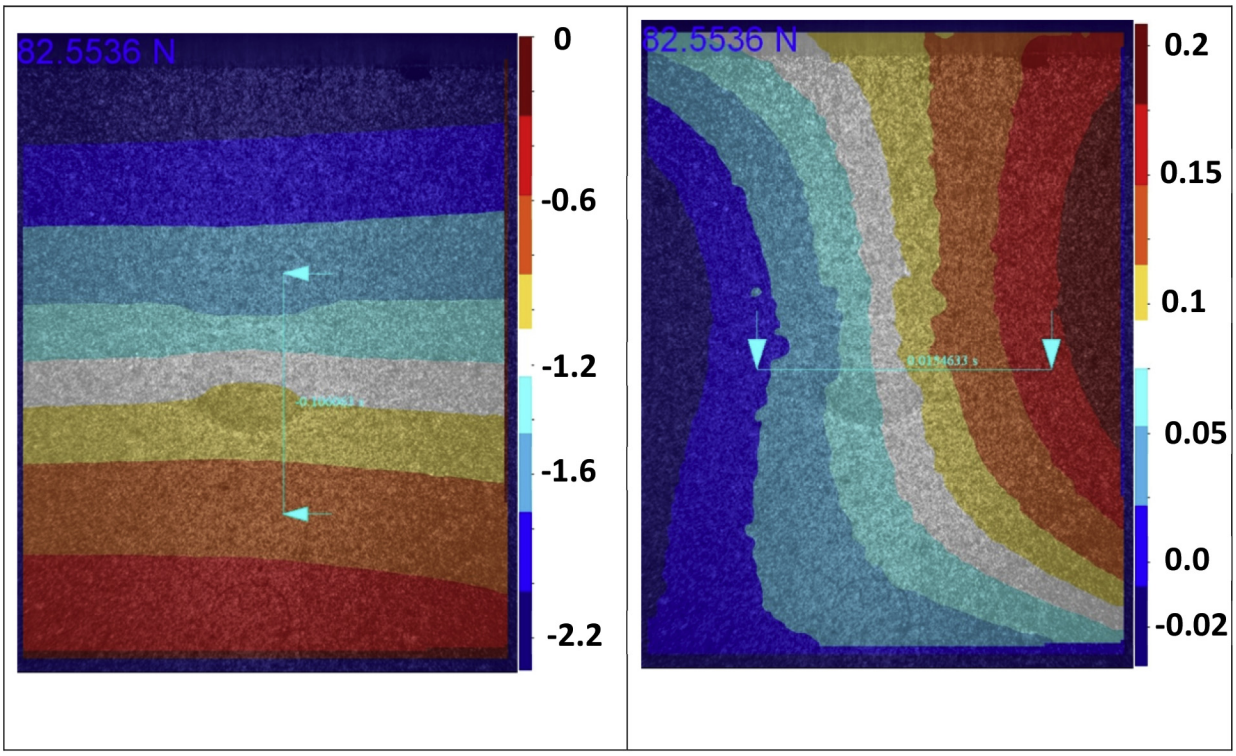

Fig. 7. Displacement fields obtained from the 2D-DIC of CAB-6 sample: (left) in the *y*-direction; (right) in the *x*-direction. Legend contours for the displacement in mm scale.

ultimate failure where the tensile stresses damage the disk at its center. Table 1 presents a summary of the converged Young's moduli for the 10 aerogel disk samples.

The block compression test is designed assuming a close to uniaxial compression state of deformation. The geometry of the aerogel block samples is not uniform and includes some manufacturing imperfections as it is hard to obtain ideal edges and surfaces. However, on average, and close to the center of the block, we anticipate a close to uniform stress and strain fields. Fig. 7 illustrates typical DIC displacement fields in a block aerogel under compression. The compressive stress is determined from the measured load divided by the area of the specific sample. Average compression (axial) and averaged transverse strains in the block samples are determined in two approaches. The first is using two vertical and horizontal virtual extensometers where their shortening and elongation can be measured from the displacements. In the second approach, the sample averaged strains are determined from the sum of the strains in a squared area around the center of the block. The typical full-field DIC displacement results shown in Fig. 7 correlate well with the anticipated linear distribution at the

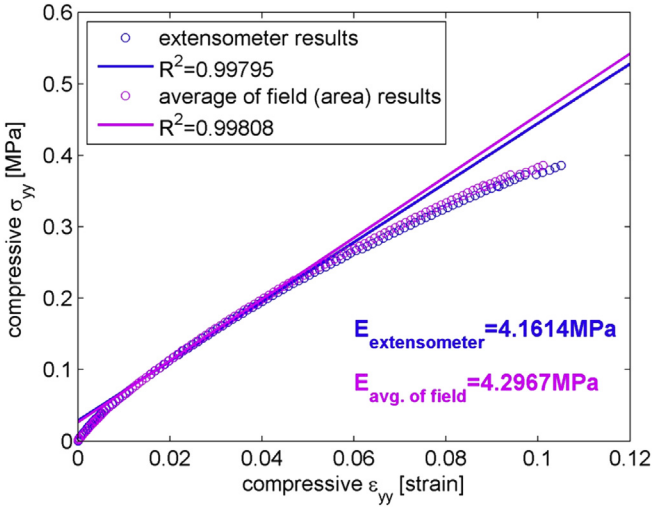

Fig. 8. Compressive stress–strain curves for CAB-6 block aerogel sample. The average stress is determined from the measured load while the strains are determined from the virtual extensometer and average DIC strains in a square area around the center of the sample. Linear regression slope lines were generated in the strain range of 0.01–0.05.

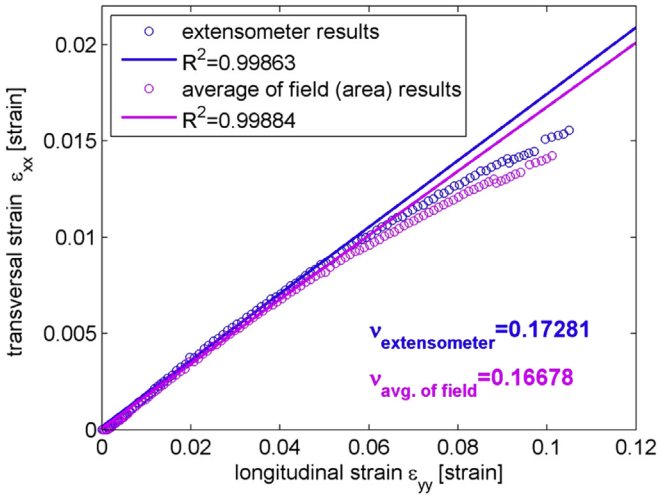

Fig. 9. Representative transverse strain versus longitudinal strain curves of CAB-6 sample. The slopes of the curves are considered as the Poisson's ratio according to the two different strain calculations. Linear regression slope lines were generated in the strain range of 0.01–0.05.

Table 2
Measured sample properties, geometry (height, width, thickness), mass and density, for six block specimens. Young's modulus and Poisson's ratio results for all six block specimens are generated using virtual extensometers and an averaged window of DIC strains. Nominal geometry reported by the manufacturer: (~2.5 cm × 2.5 cm × 1.0 cm). Error is defined as the relative deviation from nominal to measured volumes.

Specimen label	$\overline{h}$ [mm]	$\overline{w}$ [mm]	$\overline{t}$ [mm^2]	Error [%]	m [g]	ρ [g/cm^3]	E_{DIC} [MPa]	E_{VE} [MPa]	ν_{DIC}	ν_{VE}
CAB-1	24.62	24.78	8.75	14.60	0.86	0.162	1.76	1.77	0.18	0.17
CAB-2	23.77	24.06	8.43	22.87	0.85	0.177	3.81	3.87	0.19	0.19
CAB-3	23.09	23.37	8.68	25.53	1.00	0.214	5.97	6.21	0.16	0.15
CAB-4	24.02	23.91	9.21	15.40	0.98	0.185	5.60	5.900	0.18	0.17
CAB-5	23.83	23.94	9.08	17.08	0.94	0.182	5.15	5.45	0.18	0.17
CAB-6	23.93	23.95	8.87	18.65	0.94	0.185	4.16	4.30	0.17	0.17

center of the samples. Fig. 8 illustrates typical stress–strain data points and the calculated Young's modulus. A similar process is used to calculate the Poisson's ratio as the slope of the average axial compression strain when plotted against the average transverse strain, as illustrated in Fig. 9. In the case of a linear elastic material, these curves are supposed to yield linear relations; however, at the initial state a nonlinear response is shown as evident from establishing a full contact with the rigid loading plate. The nonlinear response shown in the stress–strain curve indicates an evolving damage that occurs prior to reaching ultimate failure. Table 2 lists the results for the Young's modulus and the Poisson's ratio for the six block samples, using the averaged area strains and the virtual extensometer.

Ten specimens were examined in the indirect aerogel disk tests. All of the specimens had densities ranging from approximately 150 to 200 mg/cm^3. The Young's moduli determined were in the range from 2.78 to 4.76 MPa. These are within the aerogel moduli reported for aerogels having the same range of density. Compared to Ref. [11], for example, the current results are below the reported upper bound. The Young's moduli that were obtained from the first two disk specimens are relatively smaller than the others. A reasonable explanation to this result can be related to the fact that the first two specimens were tested in the original disk fixture and may have excessive rigid body rotations during the first two tests. The elastic properties calculated from the elasticity equations assuming plane stress have smaller differences (error) compared to using the 3D-FE solution.

The direct compression testing of aerogel blocks yields the Young's moduli and Poisson's ratio in a direct manner. The Poisson's ratio is relatively independent of apparent density. Six aerogel block specimens were examined. All of the specimens had densities ranging from approximately 160 to 220 mg/cm^3. Here, the determined Young's moduli were between 1.76 and 6.21 MPa, and agreed well with the indirect disk compression method. Comparing the range of Young's moduli of the disk and block samples (Tables 1 and 2, respectively), it is noted that the Young's modulus from the block samples is somewhat on the higher bound while the disk samples give lower overall values. Noting that the samples are neither uniform in geometry nor in density, more tests are needed with different sample geometries in order to better judge the differences and scatter of the data. Finally, an average value of Poisson's ratio was found to be between 0.168 and 0.176. This supported the use of 0.2 value in the indirect test.

3.1. Limitations

The two-block compression testing of aerogels is known to be sensitive to sample size and geometry. The average height-to-thickness ratios of the two commercially available sets of block and disk compression samples were, on average, 2.72 and 3.33, respectively. The height-to-width geometric ratio in both samples is 1.0. The latter geometric ratio is small for the block samples, and a preferable ratio greater than 4 is more suitable to eliminate inhomogeneous distribution of deformation emanating from the edge areas. However, the use of the DIC method allowed extracting virtual extensometer data. In addition, a window of a close-to-uniform deformation in the block samples close to the center of the monitored areas is evident from the linear patterns of the displacement fields in Fig. 9. Nevertheless, the proposed testing methodology advocates the use of height-to-width geometrical ratio greater than 4 (assuming buckling will be prevented prior to failure). The reported results demonstrate the ability of the proposed tests to measure the mechanical properties of aerogels. The elastic modulus may have been underestimated for the block samples with smaller geometrical ratios.

4. Conclusions

The main purpose of this study was to examine two mechanical setups and testing procedures for measuring the elastic mechanical properties of (silica) aerogels; these can be used also for fracture toughness measurements. Both procedures employ full-field Digital Image Correlation (DIC) for surface deformation measurements. The first (indirect) test employs compression disk (CAD) in a Brazilian disk test, which is used here for the first time for measuring the Young's modulus of aerogels. Since the elastic properties of the material cannot be obtained directly, an inverse mechanics computational scheme, using both a finite-element (FE) model and an analytical solution, is proposed. The second (direct) test is uniaxial compression of rectangular-shaped blocks (CAB). The two setups are able to apply proper loading and can handle the material without inducing damage. The expected correlation between density and Young's modulus is found similar to values reported in the literature. The Poisson's ratio is found to be independent of the material apparent density. The DIC method is capable of providing full strain fields (not just an average stiffness) and can be used to examine material flaws due to manufacturing or damage during higher loads. The disadvantage of the CAD test setup lies in its need to employ indirect methods to extract the aerogel mechanical properties.

Acknowledgment

This work was supported by Grant No. 279/6065/99 from the Pazy Foundation of the Israeli Council of Higher Education and the Israel Atomic Energy Commission.

References

[1] J. Fricke, J. Non-Crystalline Solids 100 (1–3) (1988) 169–173.
[2] M.A. Aegerter, N. Leventis, M.M. Koebel, Aerogels Handbook, Springer, New York, 2011.
[3] A. Emmerling, R. Petricevic, A. Beck, P. Wang, H. Scheller, J. Fricke, J. Non-Crystalline Solids 185 (3) (1995) 240–248.
[4] N.a.S. Husing, U., Angew. Chem. Int. Ed. 37 (1–2) (1998) 22–45.

[5] S.M. Jones, Aerogel: space exploration applications, J. Sol-Gel Sci. Technol. 40 (2006) 351–357.
[6] H.-S. Ma, A.P. Roberts, J.H. Prévost, R. Jullien, G.W. Scherer, J. Non-Crystalline Solids 277 (2–3) (2000) 127–141.
[7] T. Woignier, J. Pelous, J. Phalippou, R. Vacher, E. Courtens, J. Non-Crystalline Solids 95–96 (Part 2(0)) (1987) 1197–1202.
[8] T. Woignier, J. Phalippou, J. Non-Crystalline Solids 100 (1–3) (1988) 404–408.
[9] T. Woignier, J. Phalippou, J. Phys. Colloq. 50 (1989) (C4).
[10] E. Courtens, J. Pelous, J. Phalippou, R. Vacher, T. Woignier, Phys. Rev. Lett. 58 (1987) 128–131.
[11] J. Gross, G. Reichenauer, J. Fricke, J. Phys. D Appl. Phys. 21 (9) (1988) 1447–1451.
[12] T. Tillotson, L. Hrubesh, J. Non-Crystalline Solids 145 (0) (1991) 44–50. Würzburg, Germany.
[13] G.W. Scherer, S.A. Pardenek, R. Swiatek, J. Non-Crystalline Solids 107 (1) (1988) 14–22.
[14] G.W. Scherer, D.M. Smith, X. Qiu, J.M. Anderson, J. Non-Crystalline Solids 186 (1995) 316–320.
[15] K.E. Parmenter, F. Milstein, J. Non-Crystalline Solids 223 (3) (1998) 179–189.
[16] M. Moner-Girona, A. Roig, E. Molins, E. Martinez, J. Esteve, Appl. Phys. Lett. 75 (5) (1999) 653–655.
[17] J.C.H. Wong, et al., Microporous Mesoporous Mater. 183 (2014) 23–29.
[18] Y.T. Sun, et al., Procedia Eng. 67 (0) (2013) 517–524.
[19] H. Luo, H. Lu, N. Leventis, Mech. Time-Depend Mater. 10 (2) (2006) 83–111.
[20] H. Luo, G. Churu, E.F. Fabrizio, et al., J. Sol-Gel Sci. Technol. 48 (2008) 113–134.
[21] A.H. Alaoui, T. Woignier, F. Pernot, J. Phalippou, A. Hihi, J. Non-Crystalline Solids 265 (1–2) (2000) 29–35.
[22] B. Pan, K. Qian, H. Xie, A. Asundi, Meas. Sci. Technol. 20 (6) (2009).
[23] W.H. Peters, W.F. Ranson, Opt. Eng. 21 (3) (1982) 427–431.
[24] H. Bruck, S. McNeill, M. Sutton, W. Peters, Exp. Mech. 29 (1989) 261–267.
[25] D.J. Chen, F.P. Chiang, Y.S. Tan, Appl. Opt. 32 (11) (1993) 1839–1849.
[26] M. Sutton, J. Yan, V. Tiwari, H. Schreier, J. Orteu, Opt. Lasers Eng. 46 (10) (2008) 746–757.
[27] Aerogel Technologies, Classic Silica™ Aerogel Monolith (Silica Aerogel), 2013. Available from: http://www.buyaerogel.com.
[28] National-instruments, NI Vision Assistant, 2005. National Instruments.
[29] LaVision, LaVision GmbH in Davis Strain Master 2D Software, 2010. Gottingen Germany.
[30] M. Mellor, I. Hawkes, Eng. Geol. 5 (3) (1971) 173–225.
[31] P. Pandey, D. Singh, Eng. Geol. 22 (3) (1986) 281–292.
[32] C. Liu, Y. Huang, M. Lovato, Int. J. Fract. 87 (3) (1997) 241–263.
[33] C. Liu, Exp. Mech. 50 (2010) 1025–1039.
[34] S. Timoshenko, Theory of Elasticity, second ed., McGraw-Hill Book Company, 1951.
[35] Abaqus, Abaqus, FE Standard, Simulia Corp, Providence, Rhode Island, USA, 2010.
[36] PixeLINK, PixeLINK Capture OEM, PixeLINK, Ottawa, ON, Canada, 2005.
[37] Vic-2D, Vic-2D, in Digital Image Correlation, Correlated Solutions, Inc., SC, USA, 2006.